CrystEngComm

Cite this: *CrystEngComm*, 2012, **14**, 875

www.rsc.org/crystengcomm

PAPER

Growth of non-branching Ag nanowires *via* ion migrational-transport controlled 3D electrodeposition†

Chunhua Ding,[a] Cuifeng Tian,[b] Ralph Krupke[c] and Jixiang Fang*[b]

Received 6th June 2011, Accepted 7th October 2011
DOI: 10.1039/c1ce05686g

Non-branching twinned Ag nanowires have been synthesized within a three-dimensional electrochemical deposition system by using a non-supporting electrolyte and an unusually high over-potential. The branching rate of the Ag nanowires is significantly decreased under the interactions of a strong applied potential and the low concentration electrolyte, in which an ion migrational-transport controlled 3D electrochemical growth is created. Additionally, according to finite-element simulations, a high density growth of Ag nanowires originating from the high over-potential creates a planar growth front, resulting in a small probability of the branching growth.

Although ramified deposits were useful in some cases, the suppression of ramification in the growth of one-dimensional (1D) nanostructures such as rods, wires, nanowires and tubes during electrodeposition was strongly desired and a persistent challenge in the last few decades.[1] Previous strategies to synthesize 1D metallic nanostructures usually need the aid of either hard templates such as anodized aluminium oxide (AAO) or softer directing agents.[2,3] Although a lot of efforts have been made to investigate the branching formation and evolution,[4,5] a significant reduction or elimination of branching under no surfactant or template-free conditions remains quite rare.

The mass transformation during electrodeposition mainly includes the processes of diffusion, migration and convection of solutes. Previous studies suggested that the branching in electrochemistry was closely relevant to the noise in transport fields. In order to suppress the noise, various approaches have been explored, such as the introduction of agarose gel into the electrolyte. While such additives made the whole experiment much more difficult to interpret. A successful strategy was reported by Wang and coworkers,[6] using an ultrathin layer electrochemical deposition (ULECD). The noise may be suppressed owing to a very thin electrolyte layer, hence a non-branching parallel filament pattern was obtained without any additives. While the correlative investigation has concentrated on the 2D electrodeposition, those in bulk-solution (3D) freestanding growth of non-branching 1D nanostructures are scarcely reported. Thus, it is intriguing to know whether the ramified feature can be suppressed within a 3D electrodeposition.

In fact, Monte Carlo simulation of electrodeposition shows that by changing the strength of electromigration, deposit morphology may vary from fractal to stringy pattern.[7] In our previous experiment, Fang *et al.* have synthesized multiply twinned Ag nanowires within a template-free electrodeposition and without any additives under a strong applied potential followed by a relaxation process.[8] In this work, we attempt to directly synthesize non-branching 1D Ag nanostructures *via* an ion migrational-transport controlled 3D electrodeposition without any additives. The branching rate of the formed Ag nanowires is significantly decreased by adjusting the concentrations of the electrolyte solution and the values of the applied potential. The growth mechanism of low branching rate of Ag nanowires is discussed.

In this experiment a simple method of electrodeposition was used to study the effect of ion electromigration on silver no-branching nanowires growth. The details of the experiment are described in the ESI† (Experimental procedure). In deionized water, under the high potential silver atoms at the anode were firstly oxidised, and then silver ions were transported to the cathode by the electric field force, at last the silver ions were reduced to silver atoms. When more silver atoms were yielded, no-branching nanowires were prepared by aggregating the silver atoms. The morphology of the Ag nanowires was investigated using scanning electron microscopy (SEM). Fig. 1(a) and (b) show SEM images of Ag nanowires obtained *via* electrodeposition for 30 min in 40 ml deionized water, which reveal that the products consist of a large quantity of wirelike nanostructures (Fig. 1(a)). In Fig. 1(b), there are scarcely any branches and many knots on the nanowires. Thus the Ag nanowires display a bamboo-like morphology. The interval between two knots

[a]*School of Aerospace, Xi'an Jiaotong University, Shann Xi, 710049, People's Republic of China*
[b]*School of Science, MOE Key Laboratory for Nonequilibrium Synthesis and Modulation of Condensed Matter, Xi'an Jiaotong University, Shann Xi, 710049, People's Republic of China. E-mail: jxfang@mail.xjtu.edu.cn; Tel: +86-29-52665995*
[c]*Karlsruhe Institut für Technologie (KIT), Institut für Nanotechnologie, Karlsruhe, 76021, Germany*

† Electronic supplementary information (ESI) available: Details of experimental procedure, TEM images (Fig. S1), simulation parameter and the calculated results (Fig. S2 and S3). See DOI: 10.1039/c1ce05686g

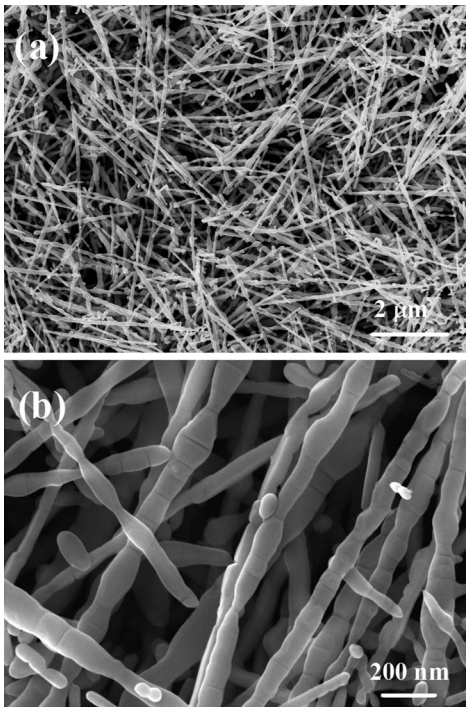

Fig. 1 SEM images of silver nanowires synthesized in deionized water under 30 V applied voltage and 30 min electrodeposition time. (a) Low-magnification image of the silver nanowires. (b) Higher-magnification image of the silver nanowires.

varies from ~10 nm to ~200 nm. The widths of Ag nanowires are approximately 100 to 150 nm.

The structure and chemical composition of Ag nanowires have been analyzed by a transmission electron microscope (TEM). Fig. 2(a) is a TEM image of the as-prepared silver nanowires, displaying the shape characteristics of the nanowires. A magnification of individual Ag nanowires and its corresponding selected area electron diffraction (SAED) pattern are shown in Fig. 2(b). As one can see from Fig. 2(b), it further reveals that each segment is single crystal and grows along the [111] direction. The crystal structure of the as-obtained nanowires (Fig. 2(c)) was investigated in more detail from the HRTEM image, showing that the twinned defect exists in the nanowire (Fig. 2(d)). The spacing of the observed lattice planes is 2.025 Å. Fig. 2(e) reveals that the SAED pattern consists of two sets of spots, and each set could be independently indexed. It can be deduced that the silver nanowires should be a twin crystal in the selected area, which is in line with previous reports for silver nanowires.[8,9] So these materials tend to grow as twinned nanowires at the (111) planes.

To find out more about the origin of branching, we analyzed the changes of morphology of Ag nanostructures under different reaction conditions. Fig. 3 shows three types of SEM micrographs of Ag nanostructures synthesized under various concentrations of $AgNO_3$ solution and different applied potentials. For the first type as shown in Fig. 3(a) and (b), the morphologies were obtained under the experimental conditions of a high potential (30 V) and a dilute solution (0.01 mM). The SEM images display that the nanowires grow out a lot of tiny bulges on the nanowires owing to relatively sufficient mass support although a high potential was employed. Its crystal structure is exhibited in Fig. S1 (ESI†). It can be seen that there is a similar twinned spot between the main backbone (shown in Fig. S1b†) and the branches (Fig. S1c†) of the nanowires. Moreover, from Fig. S1 (d)–(f)†, the spacing of lattice planes is 2.265 Å and 2.366 Å for the backbone and the branching, respectively. Therefore, it may be speculated that the nanowires are growing along the (111) planes. When the applied potential is relatively low (1 V) and

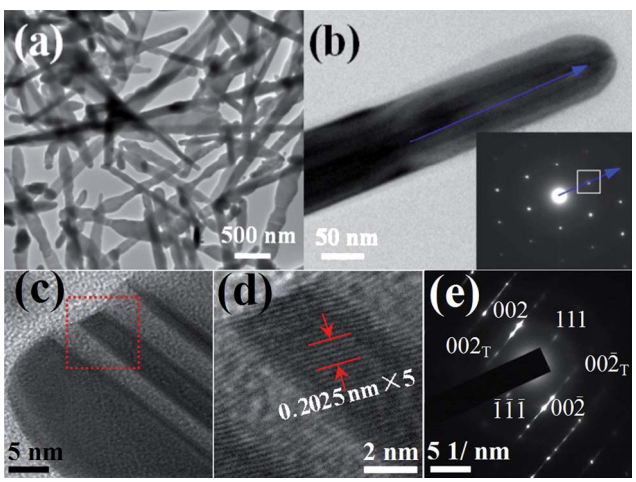

Fig. 2 (a) TEM image of silver nanowires. (b) A TEM image of an individual Ag nanowire. The inset shows its SAED pattern with a box representing the {111} Bragg reflection. (c) A magnified image of a nanowire with non-branching, and its corresponding HRTEM image and SAED pattern are shown in (d) and (e).

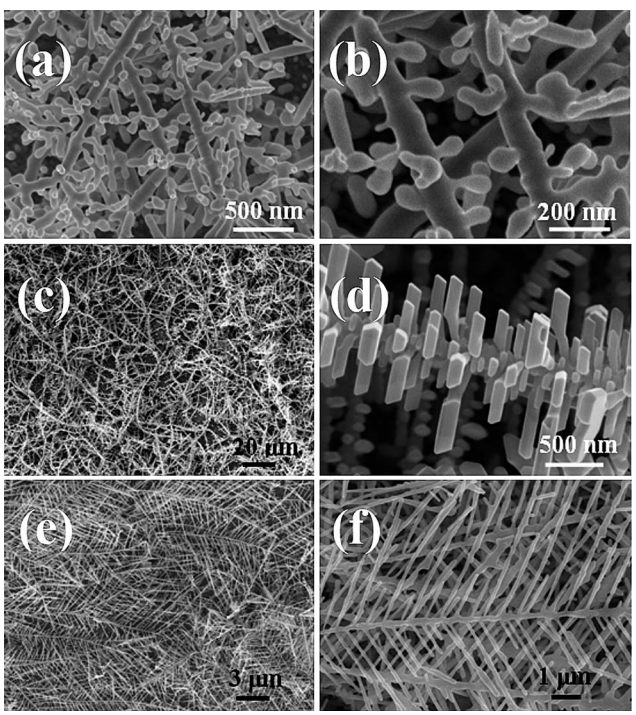

Fig. 3 Typical SEM images of Ag nanostructures synthesized under various concentrations of $AgNO_3$ solution and different applied potentials: (a and b) 0.01 mM, 30 V; (c and d) 0 mM, 1 V; (e and f) 1 mM, 30 V.

deionized water is used, the second type of morphology can be obtained as shown in Fig. 3(c) and (d) displaying many plate-like branches with the thickness about 150 nm. This is consistent with the reported tree-like structures which are obtained at low voltage and low electrolyte concentration, exhibiting the characteristics of the diffusion limited aggregation (DLA).[10] As for the third type of Ag nanostructures (Fig. 3(e) and (f)), there are still many robust branches and knots on the trunk owing to abundant solute supply from the high concentration of silver nitrate although using a high potential. At higher voltages and electrolyte concentrations, a growth transition is observed to dense-branching morphology (DBM) as reported by Matsushita *et al.*[11] At even higher voltages, dendritic aggregates appear in which crystalline anisotropy manifests itself[12] on the longest length scales.

The above results show that under a certain condition the Ag nanowires without branching can be prone to form. It is necessary to understand the growth mechanism of low branching rate during an electrodeposition. In the vicinity of the electrode, the diffusion of solute forms the concentration field. Within the concentration field, the concentration gradient initiates the convection in the vicinity of the growth front owing to the effect of gravity.[13] For a relatively high concentration electrolyte, the thickness of the diffusion layer is relatively small and the growth speed is high. Thus, the convective instability can be significant. In this case, the deposits always demonstrate a branching morphology. In contrast, when an electrochemical reaction is carried out at a relatively low concentration electrolyte, for example, deionized water in this study, the thickness of the diffusion layer is relatively large (*e.g.*, on the scale of millimetres).[14] Meanwhile, the growth, *i.e.* ion diffusion, in this case is slow. Consequently, the influence of the convection on the morphology can be relatively weak. When an unusual potential is employed combined with a low concentration electrolyte, for example, >30 V, the electromigration, the other factor that contributes to the cation transfer, may overwhelm the diffusion and the convection. Hence, the ballistic deposition will play a more important role.

The above arguments can be further supported by means of the measurement of the electrolytic conductivity. The electrical current through the electrode provides a direct measure of the flux of ions transported to the electrode surface.[15] In this study, a cathodic current was recorded during the electrodeposition process. Fig. 4(a) shows the transient current recorded for a system of deionized water under 20 V applied voltages. The increase of the current in deionized water reveals the change of the total resistance between the electrodes, and indicates that accumulation of ions takes place in the diffusion layer mainly

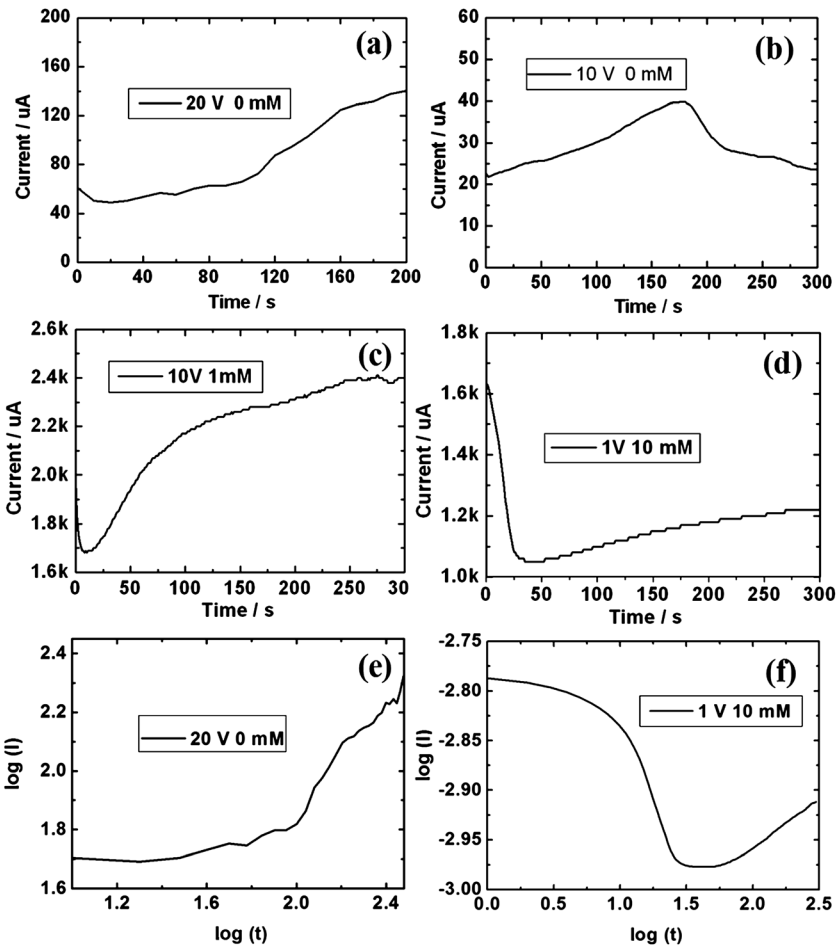

Fig. 4 Curves of current change with time for various concentrations of $AgNO_3$ solution and different external voltages: (a) 0 mM, 20 V, (b) 0 mM, 10 V, (c) 1 mM, 10 V, and (d) 10 mM, 1 V. (e) and (f) are log (*I*) *vs.* log (*t*) of scale (a) and (d), respectively.

caused by electomigration.[16] In Fig. 4(b), after approximately 178 s, the current obviously decreases from the maximum as the time increases. It can be explained that the resistance increases due to insufficient supply of ions for the growth around the cathode. In 1 mM $AgNO_3$ solution and at the same voltage, one can find that the current shows a small drop at the beginning of reaction followed by a linear increase until finally stable (Fig. 4 (c)). In this situation, the low concentration electrolyte is able to retain the electric field profile during this process. It is also implied that the ions within the diffusion layer are accommodated by migration and diffusion.[17] In Fig. 4(d) the values of current quickly decreased in the first 50 s then increased at a constant diffusion rate as the electrodeposition time increased. In this case, the mass transport of the ions through a high concentration electrolyte solution is entirely due to diffusion, except in the electric double layer (EDL) where migration may be important.[18] The current values in Fig. 4(a) compared with that in Fig. 4(d), is relatively more steady in the first 50 s. From this point, the nanowires with low branching rate can easily form in a low concentration electrolyte or deionized water electrolyte and under a high voltage. To further explain this, we plotted Fig. 4(e) and (f) as log (I) *versus* log (t) from (a) and (d), respectively. On the basis of the Cottrell equation,[19] $I = nFAC_i\sqrt{\frac{D_i}{\pi t}}$, where I is the current, A is the electrode area, C_i is the bulk concentration of the electroactive species, and D_i is its diffusion coefficient. In Fig. 4(e), it is clear that the results do not show Cottrellian behavior at short time, due to the lack of electrolyte in the solution. The reduced supplement of electrolyte also leads to a marked reduction in the conductivity of the medium and increases Ohmic drop within the solution overall, leading to "Frumkin Effects".[20] But steady increase of the current is controlled under the migration. Fig. 4(f) shows an almost linear decrease region before 31 s. Obviously, diffusion plays a main role in the transport of ions at high concentration and low voltage.

In addition to the above explanations, it is worth noting that a high nucleation density can be obtained when an electrodeposition is performed under a high potential,[21,22] which contributes to the high density growth of Ag nanowires. In this study, using the finite element solver, FlexPDE, the influence of interspaces between Ag nanowires on the branching probability is simulated (the details of simulation parameters are shown in the ESI†). Fig. 5(a) illustrates the potential distribution profile around a single Ag nanorod with a diameter of 100 nm when the interspace between nanorods exceeds 1 μm. The arrows and their colors represent the path of ion flux and their potential intensity, respectively. It is found that the potential intensity, E, around the tip of the Ag nanorod is maximal, displaying an obvious "tip" effect. When the interspace between Ag nanorods is decreased,

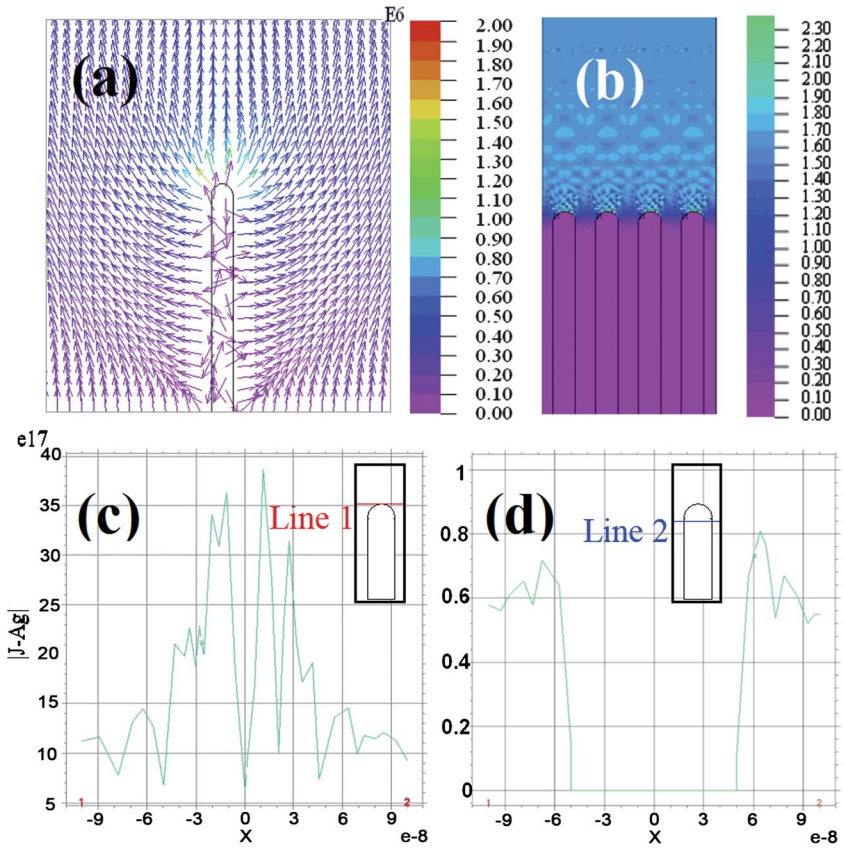

Fig. 5 Color contour plots of the magnitude of ion flux distribution for Ag nanowires arrays. (a) Electric field distribution (E), and (b) interspaces dependent-ion currents for interspaces of nanowire arrays of 100 nm. (c and d) Intensity of Ag ion flux at line 1 and line 2. Line 1: the tip of the nanorod; line 2: 50 nm below point-1.

for example, to 400, 200, and 100 nm, as shown in Fig. 5(b) and S2†, the profile of ion currents, J_{Ag+}, is significantly narrowed, demonstrating a planar growth front which results in the reduced branches of nanobelts.[23] Moreover, according to the theory of Chazalviel,[24] the cation concentration behind the growing front virtually approaches zero, which prohibits further nucleation there. If we get a deeper insight into the magnitude of ion currents, J_{Ag+}, at position 1 (tip of the nanorod) and position 2 (50 nm below position 1) which is a cross-section of a simulation for various spaced nanorods, one can find that, for a sufficiently small interspace between nanorods, the nucleation probability in the vicinity of line 2 will be much lower than that around line 1, showing a value of about 0 : 25 as indicated in Fig. 5(c) and (d). In contrast, for larger interspaces between Ag nanorods, *e.g.*, 200 nm, 400 nm and 800 nm, as shown in Fig. S3†, the nucleation probability is significantly high in the vicinity of line 2 to line 1 with a ratio of 0.6 : 25, 0.8 : 3 and 1.3 : 4. So the high nucleation density is caused by high potential and the planar growth front which results in the no-branching nanowires, resulting from the relatively dense nanorod arrays.

In conclusion, multiply twinned Ag nanowires without branches have been synthesized within a 3D electrochemical deposition system by adjusting the concentration of the electrolyte solution and the values of the applied overpotentials. Under a high voltage and in deionized water, the gravity-induced convection is successfully suppressed and the electromigration plays a significant role to create an ion migrational-transport controlled 3D electrochemical growth. Through analyzing the ion flux distribution in the vicinity of Ag nanorod arrays, it is found that an unusual high overpotential can be also very helpful for the elimination of branching attributed to high density growth of Ag nanowires and a planar profile of ion currents.

Acknowledgements

We thank Dr Haijun Jin at Karlsruhe Institute of Technology (KIT), Institute of Nanotechnology, Germany, for his helpful discussions. J. X. Fang was supported by National Natural Science Foundation of China (no. 51171139), Tengfei Talent Project of Xi'an Jiaotong University, the New Century Excellent Talents in University (NCET) and the Fundamental Research Funds for the Central Universities (no. 08142008).

References

1 H.-C. Shin, J. Dong and M. Liu, *Adv. Mater.*, 2004, **16**, 237–240.
2 Y. C. Stenphen, K. Chris and G. Jian, *Nature*, 2002, **417**, 853–857.
3 Y. G. Sun, B. Mayers, T. Herricks and Y. N. Xia, *Nano Lett.*, 2003, **3**, 955–960.
4 Z. Y. Jiang, Z. X. Xie, S. H. Zhang, S. Y. Xie, R. B. Huang and L. S. Zheng, *Chem. Phys. Lett.*, 2003, **374**, 645–649.
5 X. J. Zheng, Z. Y. Jiang, Z. X. Xie, S. H. Zhang, B. W. Mao and L. S. Zheng, *Electrochem. Commun.*, 2007, **9**, 629–631.
6 M. Wang, S. Zhong, X. B. Yin, J. M. Zhu, R. W. Peng, Y. Wang, K. Q. Zhang and N. B. Ming, *Phys. Rev. Lett.*, 2001, **86**, 3827–3830.
7 J. Erlebacher, P. C. Searson and K. Sieradzki, *Phys. Rev. Lett.*, 1993, **71**, 3311–3314.
8 J. X. Fang, H. Hahn, R. Krupke, F. Schramm, T. Scherer, B. J. Ding and X. P. Song, *Chem. Commun.*, 2009, 1130–1132.
9 Y. G. Sun and Y. N. Xia, *Adv. Mater.*, 2002, **14**, 833–837.
10 T. A. Witten and L. M. Sander, *Phys. Rev. Lett.*, 1981, **47**, 1400–1403.
11 M. Matsushita, M. Sano, Y. Hayakawa, H. Honjo and Y. Sawada, *Phys. Rev. Lett.*, 1984, **53**, 286–289.
12 D. Grier, E. Ben-Jacob, R. Clarke and L. M. Sander, *Phys. Rev. Lett.*, 1986, **56**, 1264–1267.
13 J.-N. Chazalviel, M. Rosso, E. Chassaing and V. J. Fleury, *J. Electrochem. Soc.*, 1996, **407**, 61–73.
14 S. Miyashita, Y. Saito and M. Uwaha, *J. Cryst. Growth*, 2005, **283**, 533–539.
15 D. Krapf, B. M. Quinn, M. Y. Wu, H. W. Zandbergen, C. Dekker and S. G. Lemay, *Nano Lett.*, 2006, **6**, 2531–2535.
16 C. Amatore, B. Fosset, J. Bartelt, M. R. Deakin and R. M. Wightman, *J. Electroanal. Chem.*, 1988, **256**, 255–268.
17 A. J. Bard and L. R. Faulkner, *Electrochemical Methods*, Wiley, New York, 2nd edn, 2001.
18 W. Hyk, M. Palys and Z. Stojek, *J. Electroanal. Chem.*, 1996, **415**, 13–22.
19 F. G. Z. Cottrell, *J. Phys. Chem.*, 1903, **42**, 385–431.
20 A. N. Z. Frumkin, *J. Phys. Chem.*, 1933, **164**, 121–133.
21 J. X. Fang, H. J. You, B. J. Ding and X. P. Song, *Electrochem. Commun.*, 2007, **9**, 2424–2427.
22 J. X. Fang, B. J. Ding and X. P. Song, *Appl. Phys. Lett.*, 2008, **92**, 13115–13117.
23 E. E. Mocskos, G. González, F. V. Molina and G. Marshall, *J. Electroanal. Chem.*, 2011, **653**, 27–39.
24 V. Fleury, J.-N. Chazalviel and M. Rosso, *Phys. Rev. Lett.*, 1992, **68**, 2492–2495.